# ENHANCING MIXED CONVECTION HEAT TRANSFER FROM MULTIPLE PROTRUDING HEAT SOURCES USING INCLINED OBSTACLES

تحسين إنتقال الحرارة بالحمل المختلط من عدة مصادر حرارية بارزة باستخدام عوارض مائلة

*Mahmoud. M. Awad, Gamal. I. Sultan, and Waleed. A. El-Awady*

Mechanical Power Engineering Department.
Mansoura University, Mansoura 35516, Egypt
Email: gisultan@mans.edu.eg

الخلاصة:

تم عمل دراسة معملية ونظرية لتحسين إنتقال الحرارة للأجزاء الالكترونية عن طريق توجيه الهواء الى أسطح المصادر الحرارية وفيمابينها. وتحاكى هذه الدراسة الأجزاء الأكترونية كثلاث مصادر حرارية بارزة مثبتة فى مجرى هوائى مستطيل المقطع. ويتم توجيه الهواء إلى المصادر الحرارية ومابينها باستخدام ثلاثة موجهات مثبتة على السطح العلوى لمجرى الهواء أعلى كل مصدر حرارى. وتم عمل الدراسة النظرية باستخدام أحد البرامج الجاهزة المتاحة Fluent 6.1 . ابعاد المصادر الحرارية هى ١٥ سم عرض ، ٤ سم طول ، ٢ سم ارتفاع والمسافة بين المصادر الحرارية تساوى طول المصدر الحرارى وتغير ارتفاع مجرى الهواء بين ٥,٨ الى ٩ سم بينما تغيرت زاوية ميل الموجهات لتكون ٢٦,٥° – ٣٦,٩° – ٤٥° – ٥١,٣° . وتغير رقم رينولدز مابين ٨٥٦ الى ٨٣٤٠ بينما رقم جراشوف تم تثبيته عند حوالى $2x10^7$ . وقد إمتدت الدراسة لتشمل تأثير نسبة ارتفاع النفق الى ارتفاع المصدر الحرارى بينما زاوية الميل ثبتت عند 36.9° على خصائص انتقال الحرارة. والفقد فى الضغط نتيجة بروز المصادر الحرارية وموجهات الهواء المائلة تم دراستها أيضا.

وقد بينت النتائج انه بزيادة زوايا ميل موجهات الهواء او نقص ارتفاع النفق فان انتقال الحرارة للمسخنات الثلاثة تزيد وتعطى تحسنا فى معامل انتقل الحرارة المتوسط حتى 153.14% ويزيد الفقد فى الضغط سريعا. وقد بينت النتائج ايضا أن التحسن فى معامل انتقال الحرارة المتوسط نتيجة موجهات الهواء اكبر من التحسن فى انتقال الحرارة نتيجة زيادة السرعة لنفس الطاقة المستهلكة. وتم إستنباط علاقتين لابعديتين لمعامل انتقل الحرارة المتوسط لأسطح المسخنات كدالة فى رقم ريتشاردسون ، وزاوية ميل موجهات الهواء، مع ثبات ارتفاع المجرى الهوائى وأخرى كدالة فى رقم ريتشاردسون ونسبة ارتفاع النفق الى المصدر الحرارى مع ثبات زاوية ميل موجهات الهواء عند 36.5° .

## ABSTRACT

*Experimental and numerical investigations are conducted to study the heat transfer enhancement of electronic components by re-directing the air flow to the surfaces of the heat sources and cavities between them. The study simulates the electronic components as a three heat sources which are mounted in a horizontal rectangular channel. The flow is re-directed to the heat sources using three inclined obstacles above the heat sources in order to orient the flow to both the closed cavity regions and heat sources surfaces. The numerical investigation is conducted using a commercial package "FLUENT 6.1". The heat sources dimensions are 15 cm width, 4 cm length, and 2 cm height with a spacing equals the heat source length, and channel heights of 9, 8.2, 7.4, 6.6, and 5.8 cm while the obstacles inclination angles are 26.5°, 36.9°, 45°, and 51.3°. The Reynolds number is ranged from 856 to 8340 and Grashof number is fixed at about $2.0 \times 10^7$. The study is extended to investigate the effect of channel height, at fixed inclined obstacle angle of 36.9° on heat transfer characteristics while the heat sources height is constant. The pressure drop due to heat sources protrusion and the inclined obstacles is also investigated. The results show that, as obstacle angle increases or channel height decreases (height ratio increases) the heat transfer for the three heat sources increases and gives an enhancement in the average Nusselt number up to 153.4%. It is noticed that, as the obstacle inclination angle increases the second heat source towards to have the highest heat transfer coefficient. As obstacle angle or height ratio increases, the pressure drop increases sharply. The results also show that, the enhancement of the average Nusselt number due to using obstacles angles is more than that due to increasing Reynolds number for the same consumed pumping power. Two empirical correlations for average Nusselt number as a function of Richardson number and obstacle inclination angle or height ratio are obtained for each heat source.*

Keywords: Electronic cooling, protruding heat sources, heat transfer

## 1. INTRODUCTION

During the last decades, the trend in electronic industry has been towards miniaturization, which has lead to an increase in package-level heat fluxes while the temperature limits have remained unchanged. As demands on the performance and packaging of electronic assemblies continually increase, the problem of thermal management becomes more challenging. The impact of the temperature on system reliability was shown in survey conducted by the United States Air Force, which reported that temperature is contributed to more than 50% of all electronic failure (Sergent and Al Krum [1]). Numerous experimental and numerical investigations on heat transfer enhancements in

Accepted December 20, 2006

electronic modules by using different cooling techniques, have been reported. Sathe and Sammakia [2], presented a review of recent developments in some practical aspects of air-cooled electronic packages. Habchi and Acharya [3], investigated numerically the laminar mixed convection heat transfer in a vertical channel containing a partial rectangular blockage. Rahman and Raghavan [4], carried out a numerical simulation of heat transfer during cross-flow mixed convection in electronic circuit boards. Wang and Vafai [5], presented an experimental investigation of convective heat transfer and pressure loss in a rectangular channel with discrete flush-mounted and protruding heat sources. Sultan [6], studied experimentally the forced convection heat transfer of multiple protruding heat sources with passive cooling. Iwia et al. [7], studied numerically the effect of the duct aspect ratio on heat transfer of the flow over a backward-facing step at low Reynolds number. Sparrow and Hossfeld [8], studied experimentally the effect of rounding the protruding edges on heat transfer and pressure drop. Jubran and Al-Haroun [9], studied experimentally the effect of secondary air injection hole arrangements on the heat transfer coefficient and the pressure drop characteristics. Guo and Sharif [10], simulated numerically mixed convective heat transfer in a rectangular cavity with constant heat from partially heated bottom wall while the isothermal side walls were moving in the vertical direction. Dogan et al. [11], investigated experimentally the mixed convection heat transfer in a top and bottom heated rectangular channel with discrete heat sources. Sultan [12] and Garimella and Eibeck [13], investigated experimentally the effect of spanwise spacing on the heat transfer from an array of protruding elements in forced convection. Sparrow et al. [14], investigated experimentally the effect of implemented barriers in arrays of rectangular modules and reported significant improvement in the heat transfer coefficient of the module in the second row downstream of the barrier. Garimella and Eibeck [15] studied experimentally the extent of heat transfer enhancement obtained by introducing vortex generators upstream of an inline array of heated protruding elements. Wu and Perng [16], presented a numerical investigation on heat transfer enhancement of mixed convective flow by installation of an oblique plate for internal flow modification induced by vortex shedding. Many investigations were directed to conjugate heat transfer modes, where the effects of conduction and convection heat transfer are studied [17-21]. For convective heat transfer, many different fluids are used as a working fluid. Garimella and Eibeck [22], Bhowmik et al [23] used water as a working fluid while Tso et al. [24] , Bhowmik and Tou [25] used fluorocarbons (FC-72) for a highly heat flux rate.

The aim of this work is to simulate cooling of electronic equipments experimentally and numerically to investigate mixed convective heat transfer from multiple protruding heat sources and study the effect of obstacles angle which re-direct the flow towards the surfaces of the heat sources and the cavities between heat sources. The study is extended to study the effect of channel height variation, at fixed inclination angle, on cooling of the heat sources, and pressure loss analysis is also presented.

## 2. Experimental test-rig

The schematic diagram of the experimental test-rig including the test section is shown in Figs. 1 and 2. The test section (1) of 90 cm long, with cross sectional area of 15 x 9 cm is made from wood. The air is withdrawn by the blower (19) which enters the test section through a bell mouth inlet and fine mesh screen (2) to insure uniform flow with a negligible turbulence. Three typically heat sources (4) are mounted on the base plate of the test section with spacing ratio S/L = 1. The first heat source is located at $L_1$ = 43 cm from the entrance of the channel. The heating element of each heat source is a nickel-chromium wire (5) which is wrapped at equal pitches over a ceramic core (6) of 3.5 cm length, 1.5 cm height and 15 cm width. Each core is surrounded by a 0.5 mm thickness mica-sheet (7), and is inserted inside an aluminum channel (8), 4 cm length (in the flow direction), 2 cm height, and 15 cm width to form the three protruding heat sources. Three inclined obstacles of wooden angles having different inclination (26.6°, 36.9°, 45°, 51.3°) are installed below the upper plate of the test section and above the three heat sources to re-direct the air flow to the closed cavities between each two heat sources to investigate the effect of obstacles angle on the heat transfer coefficient.

To control the heat input to each heat source and insure that each heat source emits approximately the same heat flux, each heat source is equipped with a variac transformer (10) as well as an ammeter (11), which has an accuracy of ± 0.1 A and a voltmeter (12) with an accuracy of ±1.2% of the reading. The surface temperature of each heat source is measured by nine calibrated copper-constantan thermocouples (13) which are glued well on the inside surface of the aluminum channel by means of high thermal conductivity epoxy. Also, the temperature distribution along the test section floor is measured by ten thermocouples (two thermocouples are distributed between each two heat sources, three in front of the first heat source and another three behind the last heat source). The inlet air temperature is measured by a thermocouple located at the air flow inlet. Also, the temperature above each heat source is measured by a thermocouple passing through the inclined obstacle.

1. Test section
2. Mesh screen
3. Bell mouth inlet
4. Heat sources
5. Nickel-Chromium wire
6. Ceramic core
7. Mica sheet
8. Aluminum channel
9. Thermocouples
10. Variac
11. Ammeter
12. Voltmeter
13. Thermocouples
14. Temperature recorder
15. Orifice meter
16. U-tube manometer
17. Pressure taps
18. Glass wool insulation
19. Air blowe
20. Gate plate

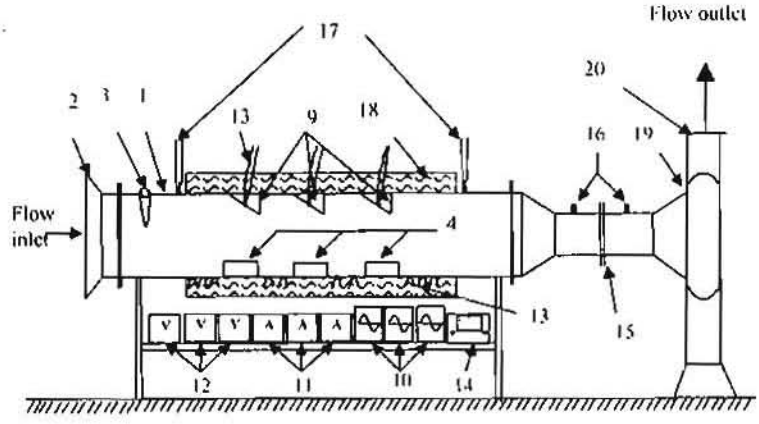


**Figure 1. Schematic diagram of the experimental test-rig**

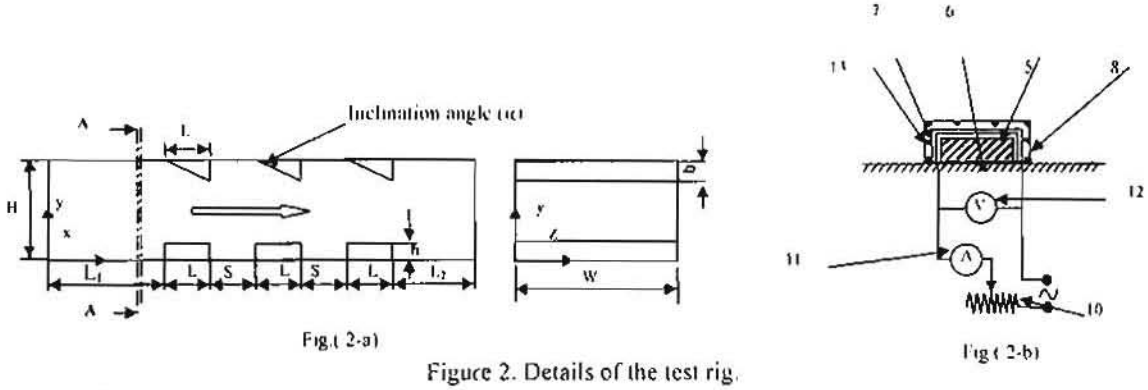


Figuce 2. Details of the test rig.

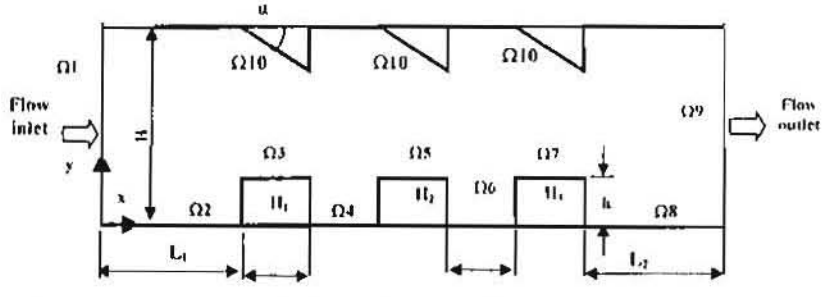


**Figure 3. Problem Physical description and boundary conditions.**

The thermocouples are connected to a digital temperature recorder (14) which has an accuracy less than ± 1% with the aid of two multi-switch points selectors.

The average flow velocity is measured by the help of an orifice meter (15) with the aid of U-tube manometer (16). The pressure drop due to the protruding heat sources and the attached inclined obstacles is measured by a U-tube manometer which connected to pressure taps (17) as shown in Fig. 1.

The test section is covered by a glass wool insulation (18) (40 mm thick) to reduce the heat loss from the test section walls to the surroundings to a negligible value.

To study the effect of channel height variation with using inclined obstacles, the channel height, H, has the values, 9.0, 8.2, 7.4, 6.6, and 5.8 cm, and the heat source height is fixed at 2 cm. These channel heights lead to height ratios, HR, of 0.222, 0.244, 0.27, 0.303, and 0.345. The angle of the inclined obstacles is fixed at 39.6° when studying the effect of height ratio. Nearly two hours are needed to reach the steady state condition, which is recorded as the temperature reading did not change with time

The connective heat flux q'' is determined from the electrical power input to each heat source using:

$$q'' = \frac{VI}{(L_s + 2h)W} \quad (1)$$

Reynolds number and Grashof number, which based on the heat source length L, are defined as:

$$Re_{L_s} = \frac{\rho_a u_m L_s}{\mu_a} \quad (2)$$

$$Gr_{L_s} = \frac{g\beta q''(L_s + 2h)L_s^3}{\lambda \nu^2} \quad (3)$$

The results are presented in terms of the dimensionless temperature $\theta_i$ , average Nusselt number, Richardson number as follow:

$$\theta_i = \left(\frac{T_i - T_a}{q'' L/\lambda}\right) Gr_{L_s}^{1/4} \quad (4)$$

The heat transfer coefficient and Nusselt number is defined as:

$$h_x = \frac{q''}{(T_s - T_a)} \quad (5)$$

$$h_{av} = \frac{1}{L_s + 2h} \int_0^{L_s+2h} h_x dx \quad (6)$$

Where $T_a$ is air temperature above the heat source, °C

$$Nu_{av} = \frac{h_{av} L_s}{\lambda} \quad (7)$$

$$Ri = \frac{Gr_{L_s}}{Re_{L_s}^2} \quad (8)$$

The friction factor and power consumed are as follow:

$$f = \frac{\Delta P_{drop}}{\frac{1}{2}\rho_a u_m^2} \quad (9)$$

$$P_c = \dot{V} \Delta P_{drop} \quad (10)$$

## 3. Numerical model

All computational results presented in this paper are obtained with the commercial CFD code FLUENT 6.1. The flow throughout computational domain is considered to be steady state, incompressible, turbulent, two-dimensional flow in the x-y plan, with constant properties.

### 3.1 Governing equations

Numerical analysis is based on the Reynolds-averaged Navier Stokes equations. The continuity, momentum, and energy equations are used as followed:

$$\frac{\partial(\rho u_j)}{\partial x_j} = 0 \quad (11)$$

$$\frac{\partial(\rho u_j u_i)}{\partial x_j} = -\frac{\partial P}{\partial x_i} + \frac{\partial}{\partial x_j}\left(\mu \frac{\partial u_i}{\partial x_j}\right) - \frac{\partial \overline{u_i' u_j'}}{\partial x_j} + \rho g_i \quad (12)$$

$$\frac{\partial(\rho u_j T)}{\partial x_j} = \frac{\partial}{\partial x_j}\left(\Gamma_t \frac{\partial T}{\partial x_j}\right) + S_t \quad (13)$$

To close the Reynolds-averaged Navier Stokes equations, the Reynolds stresses $\overline{u_i' u_j'}$ which represent the turbulence effects, are modeled using the standard k-ε model as followed:

$$\frac{\partial(\rho u_j k)}{\partial x_j} = \frac{\partial}{\partial x_j}\left[\left(\mu + \frac{\mu_t}{\sigma_k}\right)\frac{\partial k}{\partial x_j}\right] + G_k + G_b - \rho\varepsilon \quad (14)$$

$$\frac{\partial(\rho u_j \varepsilon)}{\partial x_j} = \frac{\partial}{\partial x_j}\left[\left(\mu + \frac{\mu_t}{\sigma_\varepsilon}\right)\frac{\partial \varepsilon}{\partial x_j}\right] + C_{1\varepsilon}\frac{\varepsilon}{k}(G_k + C_{3\varepsilon}G_b) - C_{2\varepsilon}\rho\frac{\varepsilon^2}{k} \quad (15)$$

$$\mu_t = \rho C_\mu \frac{k^2}{\varepsilon} \quad (16)$$

$C_{1\varepsilon}$, $C_{2\varepsilon}$ are constants, have the values as shown in table (1), and $C_{3\varepsilon}$ is calculated from the relation, [29]:

$$C_{3\varepsilon} = \tanh\left|\frac{v}{u}\right| \quad (17)$$

**Table 1. The turbulent model constants**

| $C_{1\varepsilon}$ | $C_{2\varepsilon}$ | $\sigma_k$ | $\sigma_\varepsilon$ | $Pr_t$ | $C_\mu$ |
|---|---|---|---|---|---|
| 1.44 | 1.92 | 1.3 | 0.9 | 1 | 0.09 |

The above governing equations are solved for temperature, pressure, velocity, kinetic energy (k), and dissipating rate (ε). Furthermore, the average Nusselt number, pressure drop, and stream function can be computed.

### 3.2 Problem domain

The physical description of the problem under investigation is illustrated in Fig. (3). The flow is considered two-dimensional flow in x-y plan. Protruding heat sources are represented by three blocks, 0.04 x 0.02 x 1 m, with an intermediate spacing equals

to heat source length ,placed on the floor of a rectangular channel of 1.5 m long, 1 m depth and its height varied from 0.09 to 0.058 m. The entrance channel length $L_1$ is about 0.43 m where the exit length is 0.87 m. Three inclined obstacles are presented above the three heat sources with inclination angle ranged from 0° to 51.3°.

### 3.3 Boundary conditions

The various boundaries that bounded the problem domain are illustrated in Fig. (3) and named as Ωi. Dependant variables have to be specified or its derivatives on the domain boundaries as follow:

(i) At inlet (Ω1): $0.34 \le u(0,y) \le 3.4$ m/sec, $v(0,y)=0$, $T(0,y) = 300$ K, $0.11 \le \Omega_h \le 0.165$ m, turbulent intensity = 1.15 %.

(ii) At the walls (Ωi , i=2,4,6,8, and 10): $u(x,y)= 0$ , $v(x,y)=0$, $q''=0$, $k=0$ and $\varepsilon=0$.

(iii) At the walls (Ωi, i=3,5,and 7) (heat sources top and sides surfaces): $u(x,y)=0$, $v(x,y)=0$, $q'' = 1240$ W/m$^2$, $k=0$ and $\varepsilon=0$.

(iv) At the exit (Ω9): outlet flow, the boundary conditions at the exit are adjusted (by the CFD code) such that the properties gradient at the exit equal to zero.

## 4. Results and discussions

### 4.1 Temperature distribution

The variation of local surface temperature difference along each heat sources at different Reynolds numbers ranging from 856 to 8340, constant $Gr_L=2.0\times10^7$ and spacing ratio S/L=1 is shown in Fig. (4). It is noticed that, the local surface temperature decreases with increasing Reynolds number and the surface temperature for the first heat source is less than that of the second one and the second heat source is less than the third one, for all Reynolds numbers and this agree well with Sultan [12].

Figure (5) shows the influence of Reynolds number on the maximum temperature of the three heat sources. It is clear that the maximum temperature decreases with increasing of Reynolds number and this agree well with Sultan [12].

### 4.2 Heat transfer

Figure (6) presents the behavior of the average Nusselt number with Reynolds numbers for the three heat sources. As expected, as the Reynolds number increases, the average Nusselt number for the heat sources to the fluid increases. It is clear that the first heat source has the highest Nusselt number and the third heat source has the lowest values for the studied rang of Reynolds numbers.

### 4.3 Effect of obstacle inclination angle

Figure (7) shows the effect of flow directing angle (α) on local temperature difference along the heat sources at different values of Reynolds numbers.

It is noticed that, when the flow obstacles inclination angle increases, the local temperature difference of the second heat source decreases than that of the first heat source as Reynolds number increases. Also for obstacles inclination angle (α=51.3°), the local temperature difference of the second heat source is small than the first and the third for all studied Reynolds numbers.

To show the effect of obstacles inclination angle on heat transfer coefficient, the average Nusselt number is plotted against obstacles inclination angle (α) as shown in Fig. (8).

It is noticed that, for Reynolds number, Re≤4200, the effect of inclination angle (α) is not significant for small angle α≤26.5 for the three heat sources, but for α>26.5°, a valuable increase in Nusselt number is observed. For high Reynolds numbers Re>4200, a significant increase of Nusselt number with increasing inclination angle is observed for all inclination angles. In addition, the curves show that for α≤36.9 and Re≤2345, first heat source has the highest Nusselt number. For Re ≥1480 and α≥36.9, the second heat source has the best heat transfer.

Figure (9) shows the enhancement of the average Nusselt number with respect to Reynolds number. It is observed that, at Re≤1480 and obstacles inclination angle (α=26.5), there is no enhancement of the average Nusselt number for the second and third heat sources while the average Nusselt number of the first heat source is improved. For the same obstacles inclination angle and Re>1480, all the heat sources has a valuable enhancement in the average Nusselt number. Also for the other obstacles angles, all heat sources have an improved heat transfer .

It is observed that, the maximum enhancement in average Nusselt number occurred at Re=8340 and α=51.3° for all the three heat sources: the maximum enhancement in average Nusselt number is 49.3 % for the first heat source, 102.1 % for the second heat source, and 81.6 % for the third heat source.

Figure (10) indicates the dependence of average Nusselt number of the three heat sources with Richardson number $Gr/Re^2$ for different inclination angles. In the mixed convection dominated flow, $1<Gr/Re^2<20$ [12], the average Nusselt number decreases slightly with increasing Richardson number while for forced convection dominated flow, $GR/Re^2 <1$, the average Nusselt number decrease dramatically with increasing Richardson number for all inclination angles.

### 4.4 Effect of channel height at fixed inclination angle

To study the effect of channel height at fixed inclination angle, on local surface temperature and heat transfer, five channel heights (H=90, 82, 74, 66, and 58 mm) are used. Heat sources height is kept constant at h=20 mm, which leads to height ratio (HR= h/H) of 0.222, 0.244, 0.27, 0.303, and 0.345. All heights are accomplished by inclination angle of 36.9°. Figure (11) shows the effects of channel height on local temperature difference along the heat sources at different values of Reynolds numbers. It is noticed that, the local temperature of all heat sources decrease as channel height decreases (HR increases). This decreasing may be due to the increase of the flow velocity above the heat sources as channel height decreased and the turbulent generated by the obstacles inclination angle when approaches to the heat sources surfaces. For HR= 0.222, the first heat source has the lowest surface temperature for low Reynolds numbers, and the second heat source towards to be the lowest as Reynolds number and HR increase.

To show the effect of channel height variation on heat transfer coefficient, average Nusselt number is plotted against height ratio as shown in Fig. (12). The average Nusselt number increases as Reynolds number increases and / or channel height decreases. It is noticed that, the second heat source has the best heat transfer coefficient. That is because of more turbulent generated by the obstacles angles edges. Figure (13) shows the enhancement of the average Nusselt number with respect to Reynolds number at different height ratios. It is observed that, for low Reynolds numbers (Re≤2097) and height ratios (HR=0.244 and 0.27), a valuable enhancement in heat transfer for all heat sources from 12.9% to 37.3% is observed. For height ratios (HR=0.303 and 0.304), the maximum enhancement occurred at high Reynolds numbers, the maximum enhancement in average Nusselt number occurred at Re=5864, HR=0.345 for all the three heat sources; the maximum enhancement in average Nusselt number is 79.4 % for the first heat source, 131.7 % for the second heat source, and 153.4 % for the third heat source.

### 4.5 Comparison between present experimental and numerical results

#### 4.5.1 Comparison for obstacles inclination angle variation

Figure (14) illustrates the variation of the average Nusselt number versus obstacles inclination angles at different Reynolds numbers for both experimental and numerical results.

The comparison is performed for the average Nusselt number of the heat sources top surfaces only because of the flow separation and reattachment at heat sources corners and sides. It is observed that at low Reynolds numbers and small inclination angle, there is a deviation between experimental and numerical results. The main reason of this deviation is that, the flow is in the transition region from laminar flow to turbulent flow, which agrees well with Wang and Vafai [5]. They indicated that in the presence of protrusions the critical Reynolds number, where the transition from laminar flow to turbulent flow is occurred, is between 500-2000. Nevertheless, at high Reynolds numbers and large inclination angles there is a good agreement for both experimental and theoretical results. For Re≥2345, there is a good agreement at large inclination angle ($\alpha \geq 36.9$) and for Re≥ 4200 there is a good agreement for all inclination angles.

Figure (15) illustrates the velocity profile at different obstacles inclination angles. It is noticed that, for no obstacles, the maximum velocity profile occurs away from the heat sources surfaces but when using directing obstacles, the maximum velocity moves towards the heat sources surfaces as the obstacles inclination angle increases, which depicts a reason for increasing the Nusselt number as inclination angle increases.

Figure (16) shows the effect of obstacles inclination angle on the stream lines. It is noticed that, in case of no obstacles, eddies appear between heat sources but with a large circulation (weak vorticity strength) when compared with that when using obstacles inclination angles where eddies are small (strong vorticity strength) which enhance the heat transfer from the heat sources sides as the inclination angle increases. It is also observed that, the vorticity strength increases as obstacles inclination angle increases.

#### 4.5.2 Comparison for height ratio variation

Figure (17) shows the average Nusselt number versus height ratio at different Reynolds numbers for both experimental and numerical results.

The comparison is performed for the average Nusselt number of the heat sources top surfaces. It is noticed that the present experimental and numerical data have the same trend. For the first heat source, the variation of Nusselt number with channel height is small for both results. The experimental results agree well with the numerical results at low Reynolds numbers, Re≥2345 for the first heat source and at Re≥2345 for both second and third heat sources. As Reynolds number increases, the experimental results agree well with the numerical results for both second and third heat sources, but for the first heat source, as Reynolds number and height ratio increase, the deviation is noticed. It may be due to the separation at the heat sources corners that increases as Reynolds number increases and cross sectional area above the heat source decreases, this separation leads to a large error in numerical results.

Figure (18) illustrates the velocity profile at different height ratios. It is clear that, for HR<0.27, the effect of channel height variation on velocity profile and magnitude less than that when HR>0.27 which agree with the experimental results especially for small Reynolds numbers.

Figure (19) shows the effect of channel height on the stream lines. It is noticed that, for small height ratios eddies appear between heat sources but these eddies are large (weak vorticity strength) when compared with that of large height ratios. It is also observed that, these eddies increase as height ratio increases and Reynolds number increases.

### 4.6 Pressure Drop

Although pressure drop is considered one of the most prominent and fundamental configurations related to the electronic cooling, only a few articles reported the pressure drop caused by the protruding discrete heat sources, [20]. Figures (20) and (21) depict the variation of total pressure loss coefficient with Reynolds number. It is clear that for no obstacles, the pressure loss coefficient decreases as Reynolds number increases which agree with Wang and Vafai [5]. As inclination angle or height ratio increases the pressure loss coefficient tends to be constant with Reynolds number. It may be due to the increasing of turbulent and pressure loss which increases as Reynolds number increases.

### 5.6 Comparisons between enhancement based on increasing Reynolds number and that using obstacles angles

Figures (22) show the enhancement of average Nusselt number with respect to the consumed power. It is observed that, for the first heat source, the enhancement of the average Nusselt number due to increasing of Reynolds number is better than when using obstacles angles for the same consumed power. On the other hand, the second and the third heat sources have enhancement of the average Nusselt number when using obstacles angles more than that due to increasing of Reynolds number for Re ≥4200.

Figure (23) depicts that, as the height ratio increases (channel height decreases) and obstacles inclination angle is constant ($\alpha$=36.9°). The enhancement of the average Nusselt number due to using obstacles angles is more than that due to increasing of Reynolds number for the same consumed power.

### 4-8 Correlating the experimental results

From the above discussion, it is found that, both increasing the height ratio (decreasing the channel height) and redirecting the flow towards the heat sources surfaces and cavities between heat sources increase the heat transfer coefficient. For the inclination angle variation, empirical correlations (18) are obtained to relate average Nusselt number (Nu) with Richardson number ($Gr_i/Re_i^2$) and obstacles inclination angle ($\alpha$) for each heat source as following:

$$\overline{Nu}_{1,\alpha} = 57.53\left(\frac{Gr_i}{Re_i^2}\right)^{0.26}(\cos(\alpha))^{-0.5829} \qquad (18\text{-a})$$

$$\overline{Nu}_{2,\alpha} = 52.19\left(\frac{Gr_i}{Re_i^2}\right)^{0.261}(\cos(\alpha))^{-1.1746} \qquad (18\text{-b})$$

$$\overline{Nu}_{3,\alpha} = 46.10\left(\frac{Gr_i}{Re_i^2}\right)^{0.2287}(\cos(\alpha))^{-1.1046} \qquad (18\text{-c})$$

Where subscripts 1, 2, and 3 refer to the heat source number.

The above correlations are valid for; 856 ≤Re≤8340, 0°≤$\alpha$≤53.1° and HR=0.222. Correlation (18) predicts the experimental data with an average error ±8.5 % for the first heat source, and ±14.2 % for the second and third heat sources, respectively as shown in Figs.(24-26).

For height ratio variation, empirical correlations (19) are obtained to relate average Nusselt number with Richardson number and height ratio (h/H) as following:

$$\overline{Nu}_{1,HR} = 352\left(\frac{Gr_i}{Re_i^2}\right)^{-0.2687}\left(\frac{h}{H}\right)^{1.1000} \qquad (19\text{-a})$$

$$\overline{Nu}_{2,HR} = 1057\left(\frac{Gr_i}{Re_i^2}\right)^{-0.2650}\left(\frac{h}{H}\right)^{1.3610} \qquad (19\text{-b})$$

$$\overline{Nu}_{3,HR} = 985\left(\frac{Gr_i}{Re_i^2}\right)^{-0.2370}\left(\frac{h}{H}\right)^{1.3920} \qquad (19\text{-c})$$

Correlations (19) are valid for; 856 ≤Re≤7280, 0.222≤ HR ≤0.345 and $\alpha$ =36.9° within error of ±15.5 %.

## 5. CONCLUSIONS

Mixed convective heat transfer and pressure drop for three protruding heat sources, mounted in a horizontal rectangular channel, are investigated experimentally and theoretically. The investigation is performed for obstacles inclination angles ranged from 0° to 51.3°. Reynolds numbers ranged from 856 to 8340 and constant Grashof number of approximately $2.0 \times 10^7$. The investigation is extended to include the channel-height variation while the protrusion height remains constant. From this investigation, it is conducted that:

- As obstacles angle increases the heat transfer for all heat sources increases and give an enhancement in the average Nusselt number up to 102.1%.
- Decreasing the channel height increases the heat transfer and gives an enhancement in the average Nusselt number up to 153.4 %
- For Re≤4200 and α≤26.5, the enhancement in the average Nusselt number is not significant while for Re >4200 a significant increase in the average Nusselt number is observed for all inclination angles.
- For Re ≤2097 and HR ≤0.27 a valuable enhancement in heat transfer for all heat sources, from 12.9 % to 37.3 % is observed, while at HR >0.27 the maximum enhancement occurs at Re>4200.
- As the height ratio increases and obstacles inclination angle is constant (α=36.9°), the enhancement of the average Nusselt number due to using obstacles angles is more than that due to increasing Reynolds number for the same consumed power.
- As inclination angle or height ratio increases the pressure loss coefficient tends to be constant with Reynolds number.
- Two empirical correlations, for each heat source, for average Nusselt number are obtained as shown in equations (16) and (17).

## Nomenclature

| | |
|---|---|
| b | Obstacle height, m |
| $C_\mu$ | Constant |
| $C_{1\varepsilon}$ | Constant |
| $C_{2\varepsilon}$ | Constant |
| $C_{3\varepsilon}$ | Constant |
| f | Friction factor |
| g | Gravity acceleration, m/s$^2$ |
| $g_y$ | Gravity acceleration in y direction, m/s$^2$ |
| $G_b$ | Energy generation due to buoyancy |
| $G_k$ | Turbulence kinetic energy generation |
| H | Channel height, m |
| h | Heat source height, m |
| $h_x$ | Local heat transfer coefficient, W/m$^2$.°C |
| $h_{av}$ | Average heat transfer coefficient, W/m$^2$.°C |
| I | Electrical current, A |
| k | Turbulent kinetic energy, J/kg |
| L | Heat source length in the flow direction, m |
| $L_1$ | Test section length at entrance, m |
| $L_2$ | Test section length at exit, m |
| P | Pressure, Pa |
| $P_c$ | Consumed pumping power, W |
| $P_{c,w}$ | Consumed pumping power without enhancement, W |
| $q''$ | Heat flux, W/m$^2$ |
| S | Spacing between heat sources, m |
| $S_T$ | Source term, kg/°C/m$^3$.s |
| T | Temperature, °C |
| u | Velocity in x-direction, m/s |
| u, v | Turbulent fluctuating velocities in x-direction and y-direction, respectively, m/s |
| v | Velocity in y-direction, m/s |
| V | Potential difference across heat source, V |
| $\dot{V}$ | Volume flow rate, m$^3$/s |
| W | Duct width, m |
| x, y | Cartesian co-ordinates |
| ΔP | Pressure drop across the orifice, Pa |
| $\Delta P_{d-p}$ | pressure drop across the test section, Pa |

## Dimensionless groups

| | |
|---|---|
| Gr | Grashof number, (Gr = gβq''(L+2h)L$^3$/λν$^2$) |
| Nu | Nusselt number, (Nu = hL/k) |
| Re | Reynolds number, (ρuL/μ) |
| Ri | Richardson number, (Gr/Re$^2$) |

## Greek symbols

| | |
|---|---|
| α | Obstacles inclination angle, degree |
| β | Coefficient of thermal expansion, K$^{-1}$ |
| ε | Turbulence dissipating rate, W/kg |
| θ | Dimensionless temperature difference, °C |
| ρ | Density, kg/m$^3$ |
| μ | Dynamic viscosity, N/m$^2$.s |
| Γ | Diffusion factor, kg/m.s |
| ν | Kinematic viscosity, m$^2$/s |
| λ | Thermal conductivity, W/m.°C |
| $\sigma_\varepsilon$ | Prandtl number for ε |
| $\sigma_k$ | Prandtl number for k |
| Ωi | Domain boundaries |

## Subscripts

| | |
|---|---|
| 1,α | First heat source, obstacles angle |
| 2,α | Second heat source, obstacles angle |
| 3,α | Third heat source, obstacles angle |
| 1,HR | First heat source, height ratio |
| 2,HR | Second heat source, height ratio |
| 3,HR | Second heat source, height ratio |
| a, and in | Air, inlet condition |
| av, m | average |
| e | effective |
| enh | enhancement |
| L | heat source length in the flow direction |
| max | maximum |
| Num | numerical |
| p | At constant pressure |
| t | turbulent |
| i, x | local |

## 6. REFERENCES


[1] J. E. Sergent and Al Krum, 1998. "*Thermal Management Handbook for Electronic assemblies*", McGraw-Hill Inc. New York.

[2] S. Sathe and B. Sammakia, 1998. "A Review of Recent Development in Some Practical Aspects of Air-Cooled Electronic Packages", *Journal of Heat Transfer*, Vol. 120, PP. 830-839.

[3] S. Habchi and S. Acharya, 1986, "Laminar Mixed Convection in Partially Blocked, Vertical Channel", *Int. J. Heat Mass Transfer*, Vol. 29, No. 11 , PP. 1711-1722.

[4] M. M. Rahman and J. Raghavan, 1999, "Transient Response of Protruding Electronic Modules Exposed to Horizontal Cross Flow", *International Journal of Heat and Fluid Flow*, Vol. 20, PP. 48-59.

[5] Y. Wang and K. Vafai, 1999, "Heat Transfer and Pressure Loss Characterization in a Channel With Discrete Flush-Mounted and Protruding Heat Sources", *Experimental Heat Transfer*, Vol. 12, PP. 1-16.

[6] G. I. Sultan, 2000, "Enhancing Forced Convection Heat Transfer from Multiple Protruding Heat Sources Simulating Electronic Components in a Horizontal Channel by Passive Cooling", *Microelectronics Journal* Vol. 31, PP. 773-779.

[7] H. Iwai, K. Nakabe, and K. Suzuki, 2000, "Flow and Heat Transfer Characteristics of Backward-Facing Step Laminar Flow in a Rectangular Duct", *Int. J. Heat Mass Transfer*, Vol. 43, PP. 457-471.

[8] E. M. Sparrow and L. M. Hossfeld, 1984, " Effect of Rounding of Protruding Edges on Heat Transfer and Pressure Drop in a Duct", *Int. J. Heat Mass Transfer*, Vol. 27, No. 10, PP. 1715-1723.

[9] B. A. Jubran and M. S. Al-Haroun, 1998, "Heat Transfer Enhancement in Electronic Modules Using Various Secondary Air Injection Hole Arrangements" , *Journal of Heat Transfer*, Vol. 120, PP. 342-347.

[10] G. Guo and M. A. R. Sharif, 2004, "Mixed Convection in Rectangular Cavities at Various Aspect Ratios with Moving Isothermal Sidewalls and Constant Flux Heat Source on The Bottom Wall", *International Journal of Thermal Sciences*, Vol. 43 , PP. 465-475.

[11] A. Dogan, M. Sivrioglu, and S. Baskaya, 2005, "Experimental Investigation of Mixed Convection Heat Transfer in a Rectangular Channel With Discrete Heat Sources at the Top and The Bottom", *International communication in Heat and Mass Transfer* Vol. 32, PP. 1244-1252.

[12] G. I. Sultan, 1999, "Mixed Convection Cooling of Multiple Protruding Heat Sources in a Horizontal Channel", *Mansoura Eng. Journal (MEJ)*, Vol. 24, No. 3.

[13] S. V. Garimella and P. A. Eibeck, 1991, "Effect of Spanwise Spacing on The Heat Transfer from an Array of Protruding Elements in Forced Convection", *Int. J. Heat Mass Transfer*, Vol. 34, No. 9, PP. 2427-2430.

[16] E. M. Sparrow, S. B. Vemuri and D. S. Kadle, 1983, "Enhanced and Local Heat Transfer, Pressure Drop, and Flow Visualization for Arrays of Block-Like Electronic Components", *Int. J. Heat Mass Transfer*, Vol. 26, No. 5, PP. 689-699.

[17] S. V. Garimella and P. A. Eibeck, 1991, " Enhancement of Single Phase Convective Heat Transfer from Protruding Elements Using Vortex Generators", *Int. J. Heat Mass Transfer*, Vol. 34, No. 9, PP. 2431-2433.

[18] H. W. Wu and S. W. Perng, 1999, "Effect of an Oblique Plate on Heat Transfer Enhancement of Mixed Convection Over Heated Blocks in a Horizontal Channel", *Int. J. Heat Mass Transfer* Vol 42, PP. 1217-1235.

[19] S. Y. Kim, H. J. Sung, and J. M. Hyun, 1992, "Mixed Convection from Multiple-Layered Boards with Cross Streamwise Periodic Boundary Conditions", *Int. J Heat Mass Transfer*, Vol. 35, No. 11, PP. 2941-2952.

[20] S. H. Kim and N. K. Anand, 1994, "Turbulent Heat Transfer Between a Series of Parallel Plates with Surface -Mounted Discrete Heat Sources", *Journal of Heat Transfer*, Vol.116, PP. 577-587.

[21] R. Sugavanam, A. Ortaga, and C. Y. Choi, 1994, "A Numerical Investigation of Conjugate Heat Transfer from a Flush Heat Source on a Conductive Board in Laminar Channel Flow", *Intersociety Conference on Thermal Phenomenon*.

[22] W. Nakayama, And S. H. Park, 1996, "Conjugate Heat Transfer from a Single Surface-Mounted Block to Forced Air Flow in a Channel", *Journal of Heat Transfer*, Vol. 118, PP. 301-309.

[23] P. N. Madhavan and V. M. K. Sastri, 2000, " Conjugate Natural Convection Cooling of Protruding Heat Sources Mounted on a Substrate Placed Inside an Enclosure: a Parametric Study", *Comput. Methods Appl Mech. Engrg.* 188 PP. 187-202.

[24] S. V. Garimella and P. A. Eibeck, 1990, " Heat Transfer Characteristics of Array of Protruding Elements in Single Phase Forced Convection", *Int J. Heat Mass Transfer*, Vol. 33, No. 12, PP. 2659-2669.

[25] H. Bhowmik, C. P. Tso, K. W. Tou, and F. L. Tan, 2005, "Convection Heat Transfer from Discrete Heat Sources in a Liquid Cooled Rectangular Channel", *Applied Thermal Engineering*, Vol. 25, PP. 2532-2542.

[26] C. P. Tso, K. W. Tou, and G. P. Xu, 2000, " Flow Boiling Critical Heat Flux of Fc-72 from Flush-Mounted and Protruded Simulated Chips in a Vertical Rectangular Channel", *International journal of Multiphase Flow*, Vol. 26, PP. 351-365.

[27] H. Bhowmik and K. W. Tou, 2005, "Study of Transient Forced Convection Heat Transfer from Discrete Heat Sources in a Fc-72 Cooled Vertical Channel", *International Journal of Thermal Sciences*, Vol. 44 , PP. 499-505.

[28] FLUENT version 6.1, 2003, "*user's Manual Guide*".

[29] S. V. Patanker, 1980, "*Numerical Heat Transfer and Fluid Flow*", McGraw-Hill, New York.

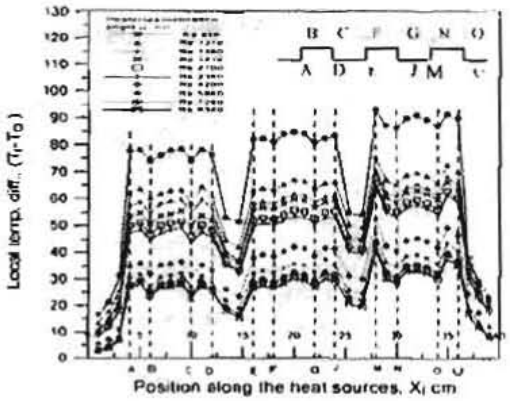


Fig. 4 Variation of local surface temperature difference with x, at different Reynolds numbers for $\alpha$=0.0°, HR= 0.222, $Gr_L$ =2.0x10$^7$.

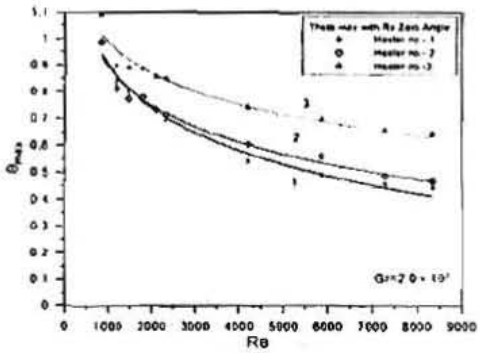


Figure 5. Variation of maximum surface temperature of heat sources with Reynolds number for $\alpha$=0.0°, HR= 0.222.

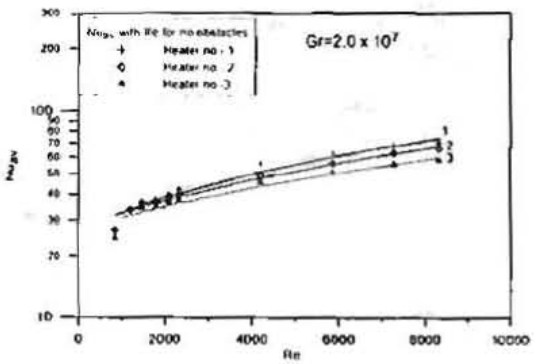


Figure 6 The average Nusselt number of heat sources versus Reynolds number for $\alpha$=0.0, HR= 0.222.

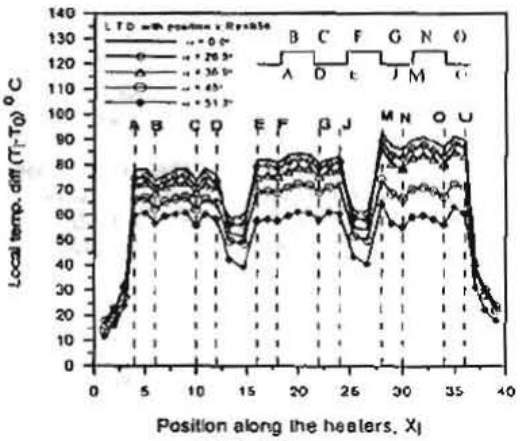


(a) Re=856.

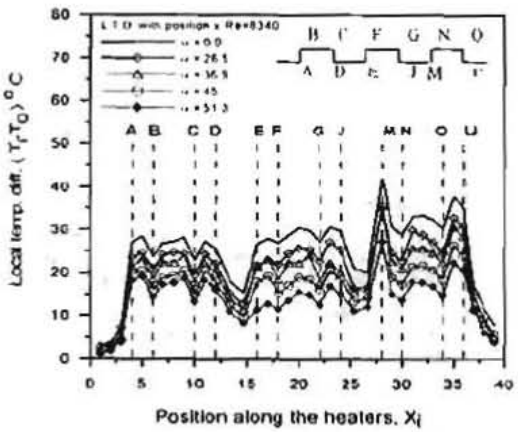


(b) Re=8340

Figure 7. The local surface temperature difference versus $x_i$ at different Reynolds numbers and inclination angles, HR=0.222, $Gr_L$ =2.0 x 10$^7$

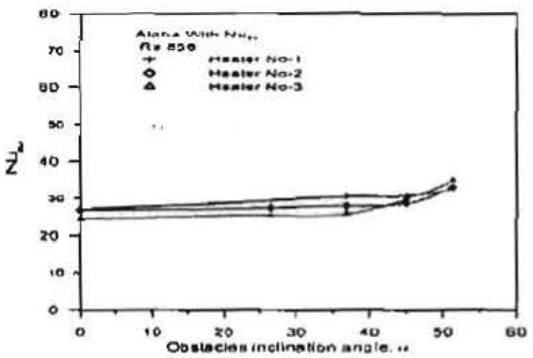


(A)

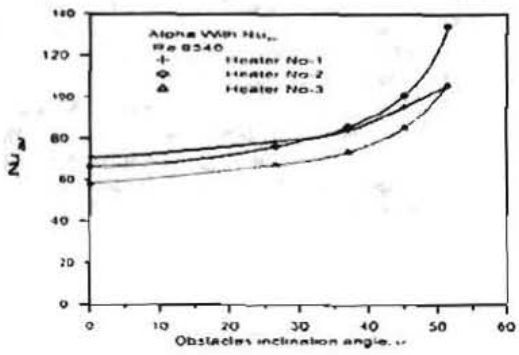


(B)

Figure 8. The average Nusselt number of the three heat sources versus obstacles inclination angle at different Reynolds numbers, $Gr_L$=2x10$^7$, HR= 0.222.

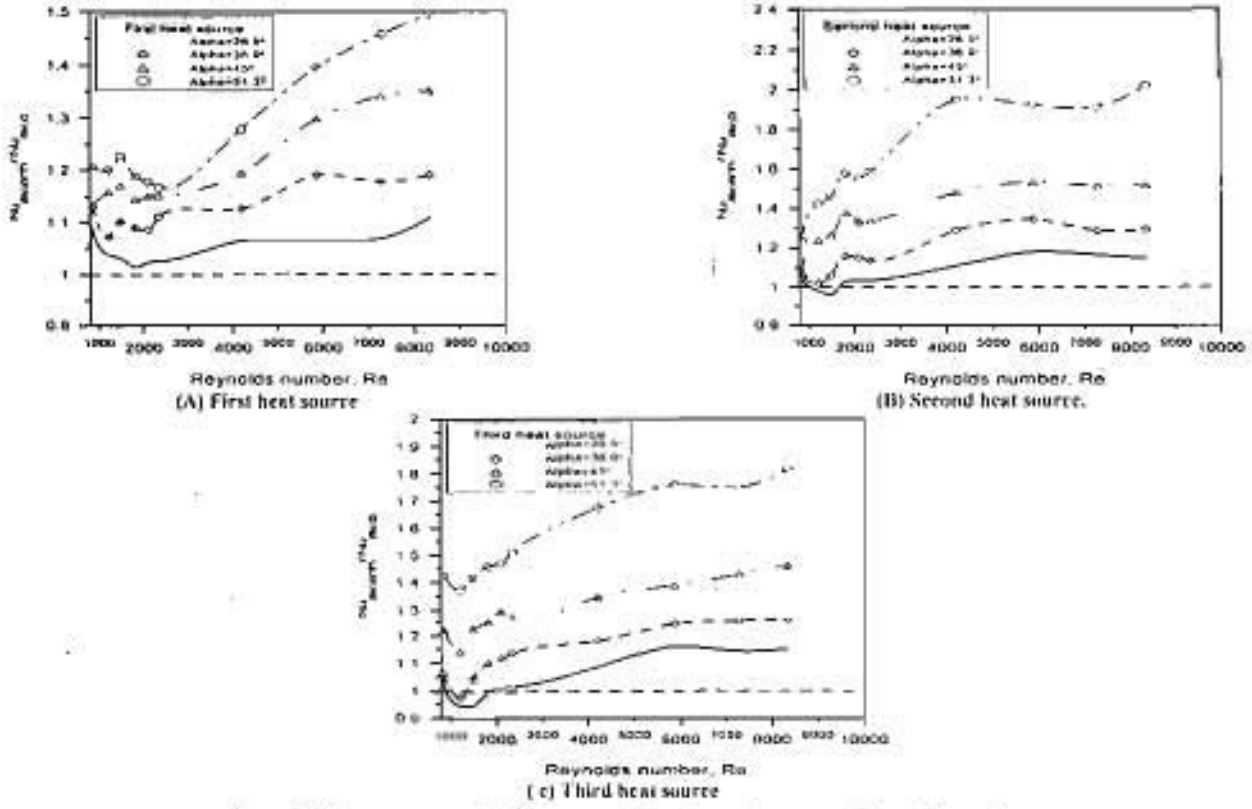


Figure 9. Enhancement ratio of the average Nusselt number versus Reynolds number at different obstacles inclination angles. $Gr_L$=2x107. HR= 0.222.

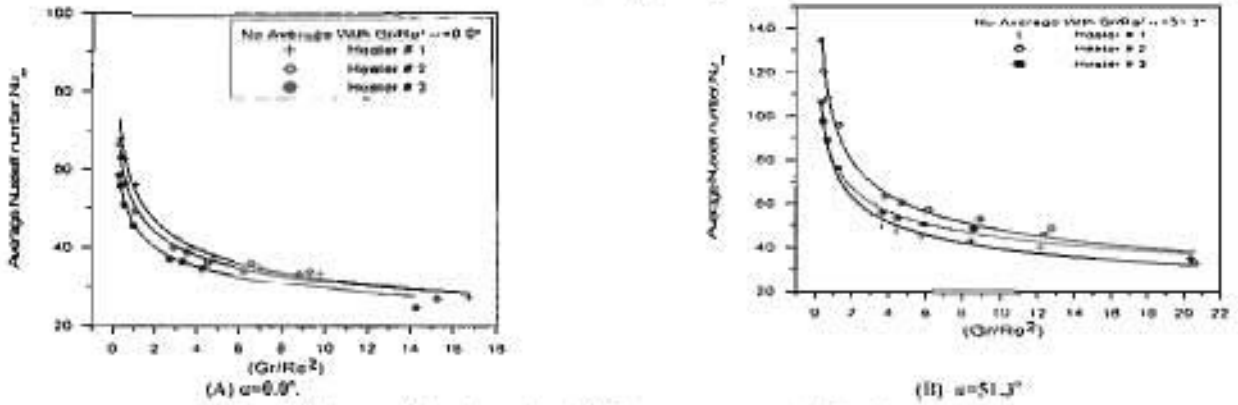


Figure10. Average Nusselt number of the heat sources versus Richardson number for diff. obstacles inclination angles. HR=0.222. $Gr_L$ = 2.0x $10^7$.

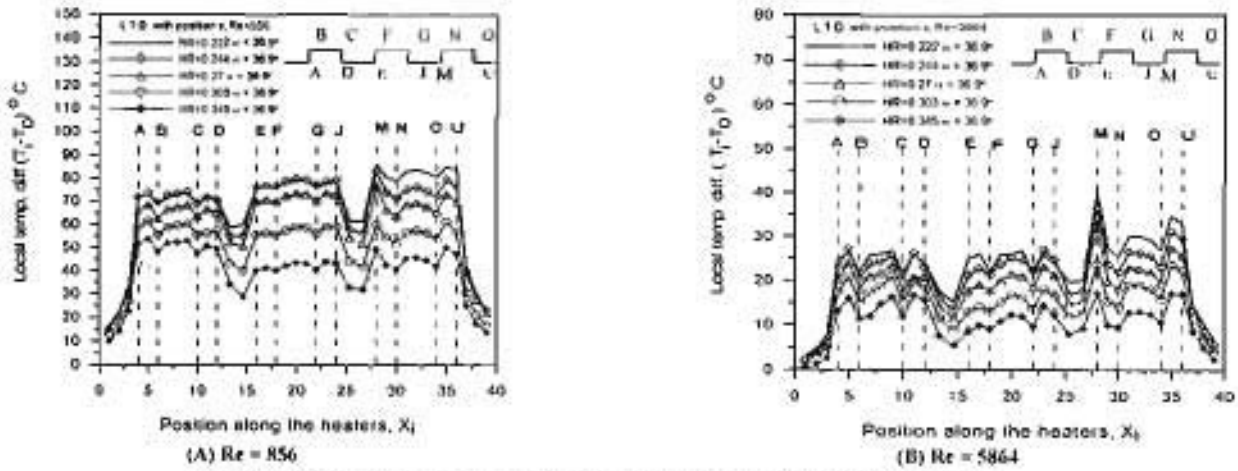


Figure 11. The variation of local surface temp. diff. with x, at diff. Reynolds numbers and height ratio at fixed inclination angle of 36.9°. $Gr_L$ =2.0 x $10^7$.

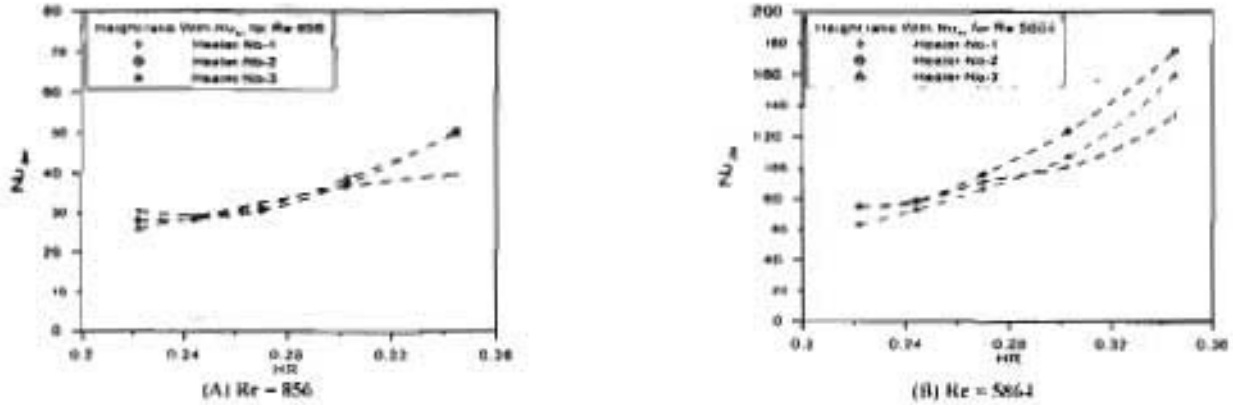

(A) Re = 856 (B) Re = 5864

Figure 12. The average Nusselt number of the heat sources versus height ratio at diff. Reynolds numbers, $\alpha$=36.9°

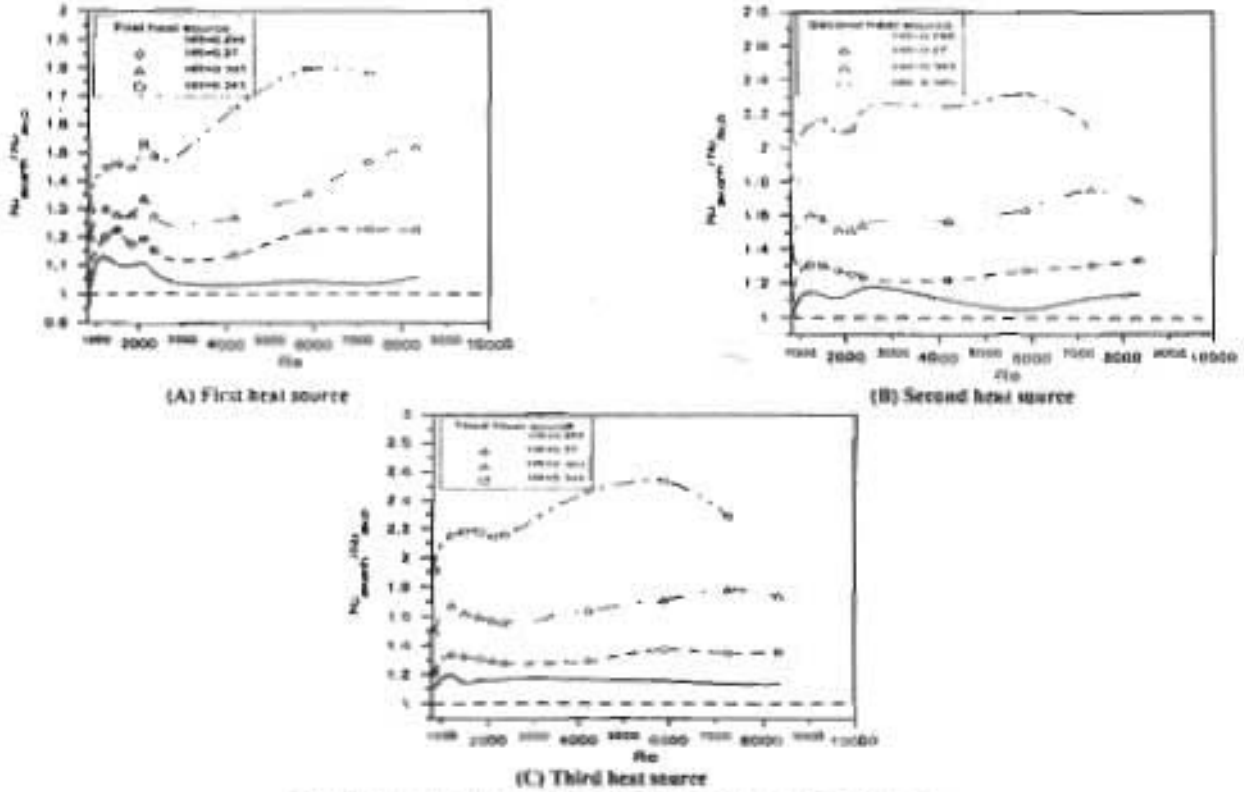

(A) First heat source (B) Second heat source

(C) Third heat source

Figure 13. Enhancement ratio of the average Nusselt number versus Reynolds number at different height ratios, $\alpha$=36.9°

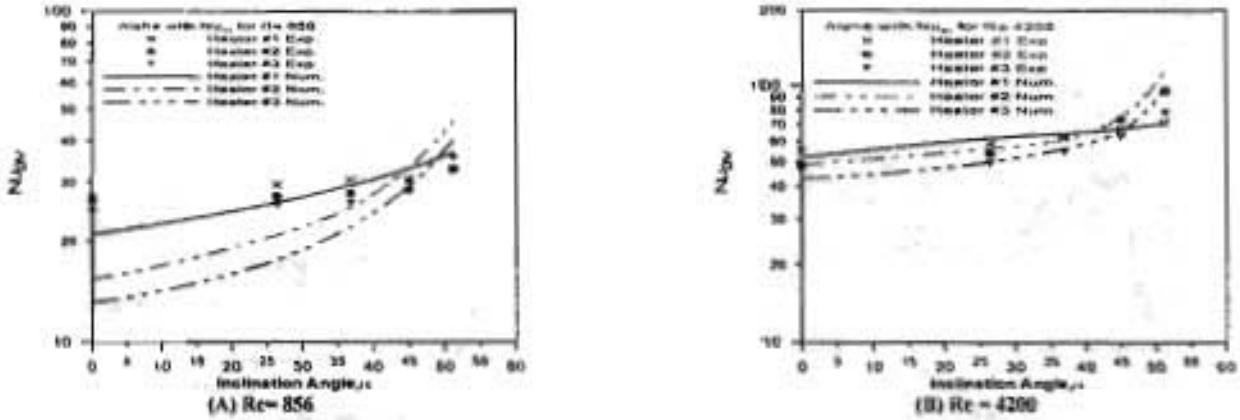

(A) Re= 856 (B) Re = 4200

Figure 14. Comparison between experimental and numerical results for the average Nusselt number of the heat sources versus inclination angle at different Reynolds numbers.

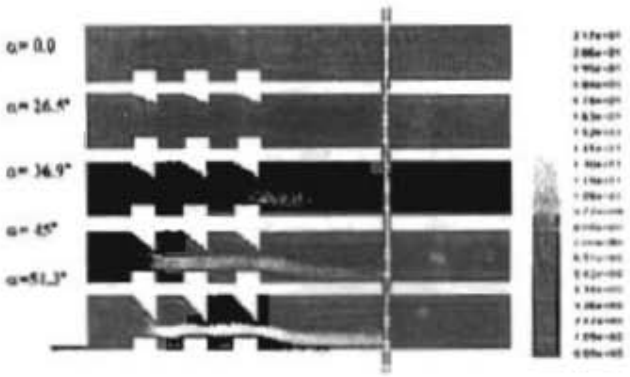

Figure 15 Velocity distribution (m/s) for Re = 8340 at different inclination angels.

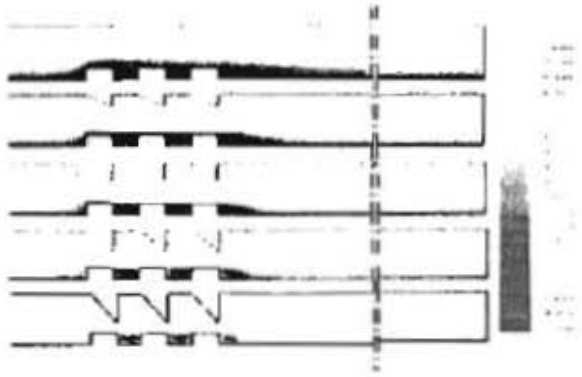

Figure 16 Stream function distribution (kg/s) for Re = 8340 at different inclination angels.

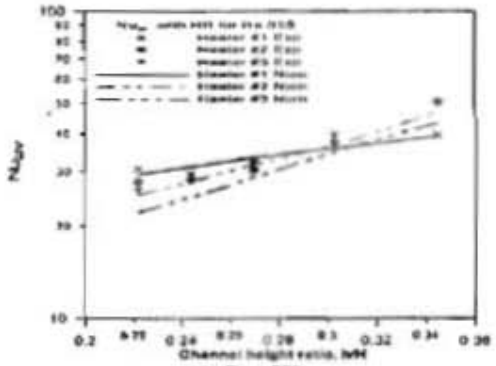

(A) Re = 856

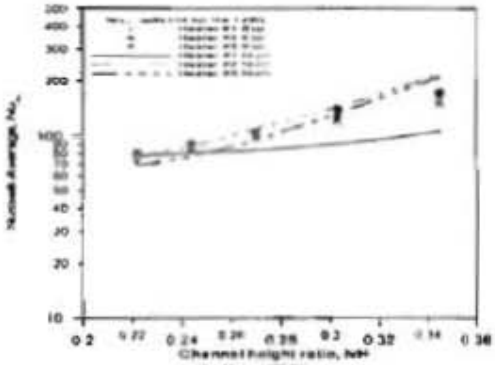

(B) Re = 7280

Figure 17 Comparison between experimental and numerical results of the average Nusselt number for the heat sources versus height ratio at different Reynolds numbers.

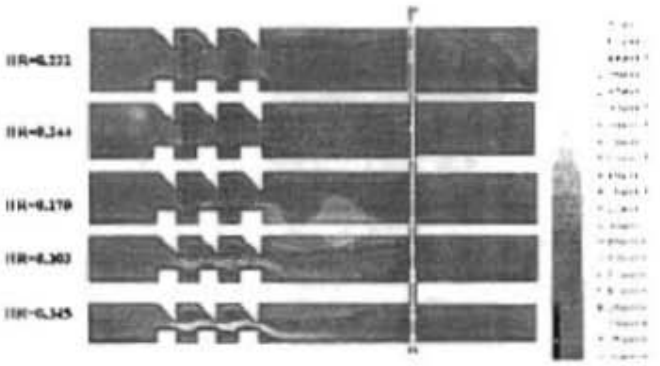

Fig.18 Velocity distribution for Re=7280 m/s at different height ratios.

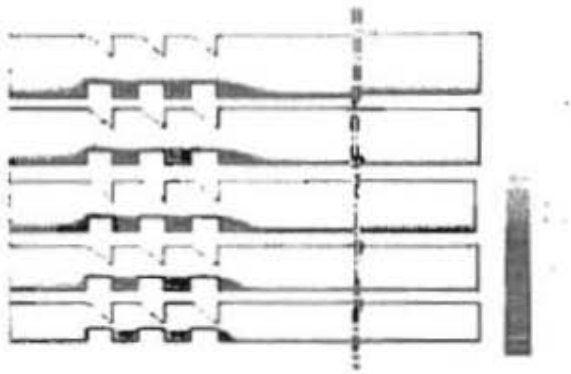

Figure 19. Stream function (kg/s) distribution for Re = 7280 at different height ratios.

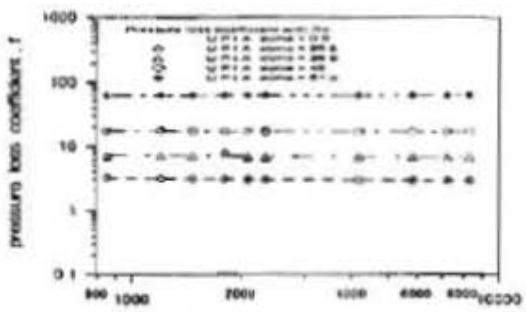

Figure 20. Pressure loss coefficient versus Reynolds number at different inclination angles (numerical results).

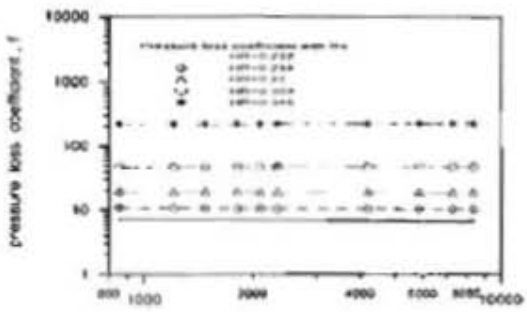

Figure 21 Pressure loss coefficient versus Reynolds number at different height ratios (numerical results).

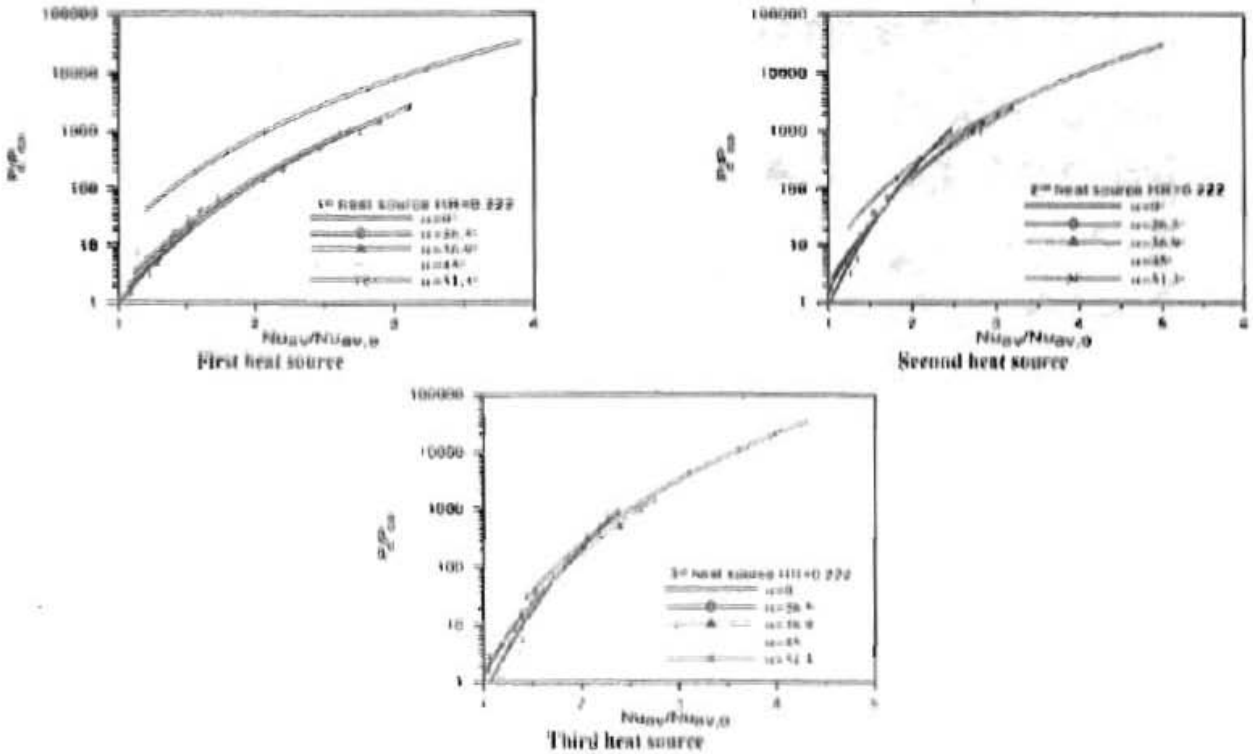


Figure 22. Consumed power ratio versus average Nusselt number ratio at different obstacles inclination angles.

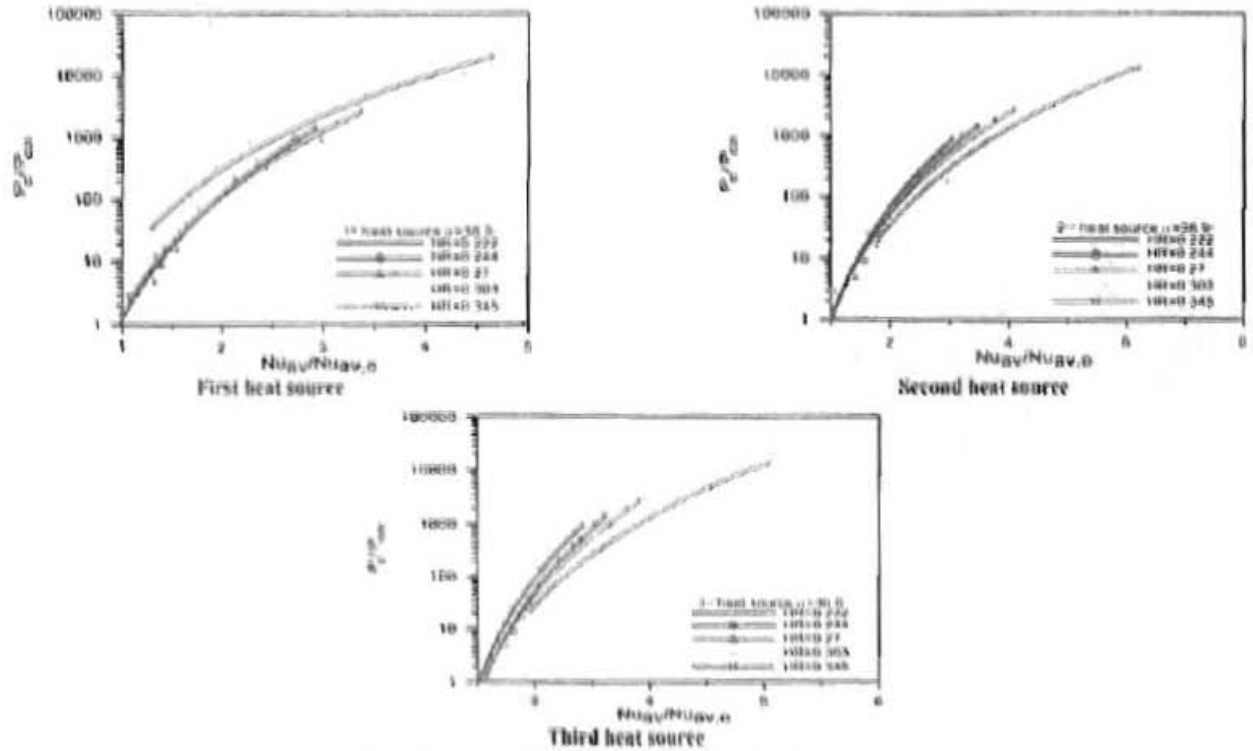


Figure 23. Consumed power ratio versus average Nusselt number ratio at different height ratios.

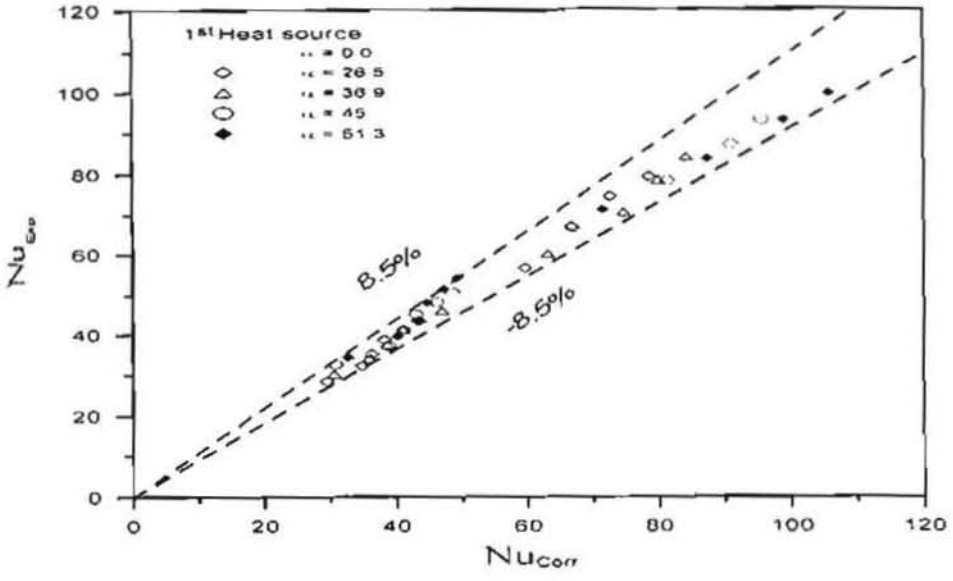


Figure 24 Deviation of experimental results of Nusselt number from correlations (18) for the first heat source.

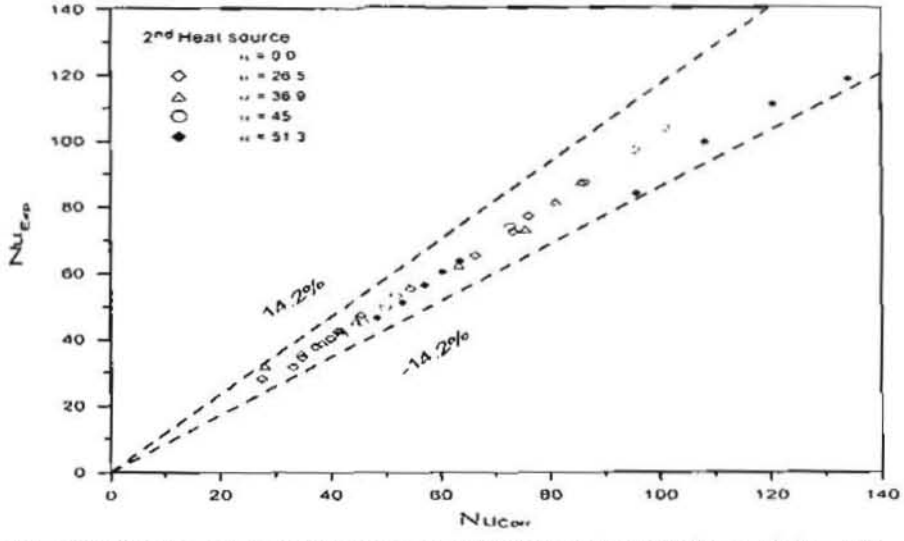


Figure 25 Deviation of the experimental results of Nusselt number from the correlations (18) for the second heat source.

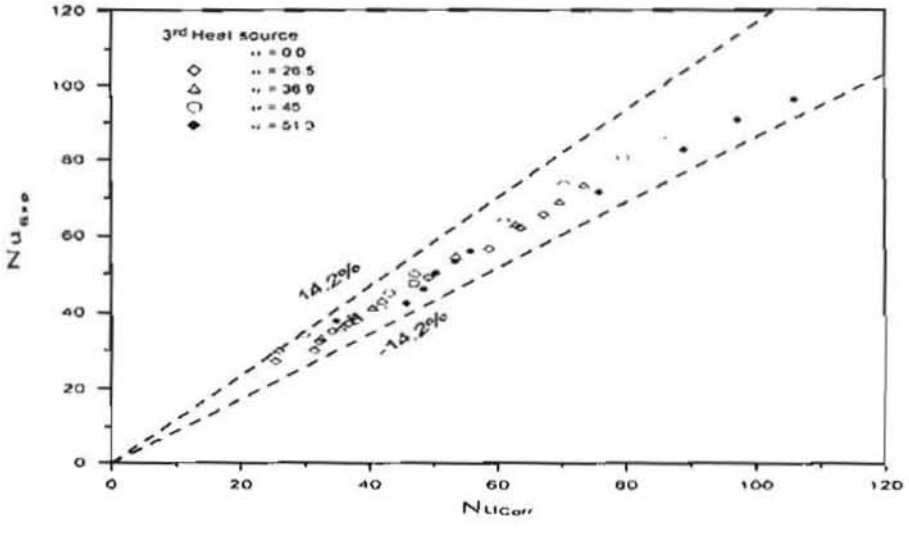


Figure 26 Deviation of the experimental results of Nusselt number from the correlations (18) for the third heat source.